

B fields in OB stars (BOB):

Detection of a strong magnetic field in the O9.7 V star HD 54879^{*}

N. Castro¹, L. Fossati¹, S. Hubrig², S. Simón-Díaz^{3,4}, M. Schöller⁵, I. Ilyin², T. A. Carrol², N. Langer¹, T. Morel⁶,
F. R. N. Schneider^{1,7}, N. Przybilla⁸, A. Herrero^{3,4}, A. de Koter^{9,10}, L. M. Oskinova¹¹, A. Reisenegger¹², H. Sana¹³ and
the BOB collaboration

¹ Argelander-Institut für Astronomie der Universität Bonn, Auf dem Hügel 71, 53121, Bonn, Germany
e-mail: norberto@astro.uni-bonn.de

² Leibniz-Institut für Astrophysik Potsdam (AIP), An der Sternwarte 16, D-14482 Potsdam, Germany

³ Instituto de Astrofísica de Canarias, 38200, La Laguna, Tenerife, Spain

⁴ Universidad de La Laguna, 38205, La Laguna, Tenerife, Spain

⁵ European Southern Observatory, Karl-Schwarzschild-Str. 2, 85748 Garching bei München, Germany

⁶ Institut d'Astrophysique et de Géophysique, Université de Liège, Allée du 6 Août, Bât. B5c, 4000, Liège, Belgium

⁷ Department of Physics, University of Oxford, Denys Wilkinson Building, Keble Road, Oxford OX1 3RH, United Kingdom

⁸ Institut für Astro- und Teilchenphysik, Universität Innsbruck, Technikerstr. 25/8, 6020, Innsbruck, Austria

⁹ Astronomical Institute Anton Pannekoek, University of Amsterdam, Kruislaan 403, 1098 SJ, Amsterdam, The Netherlands

¹⁰ Instituut voor Sterrenkunde, KU Leuven, Celestijnenlaan 200D, 3001 Leuven, Belgium

¹¹ Institute for Physics and Astronomy, University of Potsdam, D-14476 Potsdam, Germany

¹² Instituto de Astrofísica, Pontificia Universidad Católica de Chile, Casilla 306, Santiago 22, Chile

¹³ European Space Agency, Space Telescope Science Institute, 3700 San Martin Drive, Baltimore, MD 21218, USA

Received –; accepted –

ABSTRACT

The number of magnetic stars detected among massive stars is small; nevertheless, the role played by the magnetic field in stellar evolution cannot be disregarded. Links between line profile variability, enhancements/depletions of surface chemical abundances, and magnetic fields have been identified for low-mass B-stars, but for the O-type domain this is almost unexplored. Based on FORS 2 and HARPS spectropolarimetric data, we present the first detection of a magnetic field in HD 54879, a single slowly rotating O9.7 V star. Using two independent and different techniques we obtained the firm detection of a surface average longitudinal magnetic field with a maximum amplitude of about 600 G, in modulus. A quantitative spectroscopic analysis of the star with the stellar atmosphere code FASTWIND results in an effective temperature and a surface gravity of 33000 ± 1000 K and 4.0 ± 0.1 dex. The abundances of carbon, nitrogen, oxygen, silicon, and magnesium are found to be slightly lower than solar, but compatible within the errors. We investigate line-profile variability in HD 54879 by complementing our spectra with spectroscopic data from other recent OB-star surveys. The photospheric lines remain constant in shape between 2009 and 2014, although H α shows a variable emission. The H α emission is too strong for a standard O9.7 V and is probably linked to the magnetic field and the presence of circumstellar material. Its normal chemical composition and the absence of photospheric line profile variations make HD 54879 the most strongly magnetic, non-variable single O-star detected to date.

Key words. Stars: atmospheres – Stars: evolution – Stars: magnetic field – Stars: massive – Stars: individual: HD 54879

1. Introduction

The nature and role of magnetic fields in massive stars is currently poorly understood (Maeder & Meynet 2000; Ud-Doula et al. 2009; Briquet et al. 2012; Langer 2012). The origin of magnetic fields in main-sequence stars in the upper part of the Hertzsprung-Russell diagram (HRD) is being debated (Moss 2001; Ferrario et al. 2009; Tutukov & Fedorova 2010; Langer 2014; Wickramasinghe et al. 2014) and the role that these fields play in stellar evolution is being explored (Langer 2012).

The properties of magnetic fields in intermediate mass stars (A and late-B stars) have been studied in detail (see Landstreet 1992; Kochukhov & Bagnulo 2006; Hubrig et al. 2007; Donati & Landstreet 2009, and references therein), presenting links be-

tween the magnetic field strength, chemical peculiarities, and age (Ap/Bp stars, Borra & Landstreet 1980; Landstreet et al. 2007, 2008; Bailey et al. 2014). However, magnetism in the upper part of the HRD is poorly understood (Donati & Landstreet 2009; Langer 2012; Martins et al. 2012a). Magnetic fields have been unambiguously detected only in a few dozen main-sequence O- and B-type stars (see e.g. Briquet et al. 2013; Petit et al. 2013; Alecian et al. 2014; Fossati et al. 2014, 2015; Hubrig et al. 2014b; Neiner et al. 2014, and references therein), revealing a small magnetic field incidence of 7% (Wade et al. 2014; Morel et al. 2015). In the O-star subsample, the confirmed magnetic field detections are even scarcer; only ten stars have been reported (Donati et al. 2002, 2006; Bouret et al. 2008; Hubrig et al. 2008; Grunhut et al. 2009; Martins et al. 2010; Hubrig et al. 2011; Nazé et al. 2012; Wade et al. 2012a,b; Grunhut et al.

^{*} Based on observations made with ESO telescopes at the La Silla and Paranal observatories under programme ID 191.D-0255(C,F).

2013), most of them classified as Of?p stars or peculiar¹ in some other way (e.g. θ^1 Ori C is a well-known variable star).

A larger number of detections is mandatory to find links between stellar parameters and magnetic fields. The “B fields in OB stars” (BOB) collaboration methodically searches for magnetic fields in slowly rotating, massive main-sequence stars (Morel et al. 2014, 2015). The first results from the BOB project have been published by Hubrig et al. (2014b, 2015) and Fossati et al. (2015).

We present here the first detection of a strong magnetic field in the star HD 54879 and the quantitative characterisation of its optical spectrum. HD 54879 ($V = 7.65$, Reed 2003) is an O9.7 V star (Sota et al. 2011) and a probable member of the CMa OB1 association, which is about 3 Myr old (Clariá 1974), at a distance of $\sim 1320 \pm 130$ pc (Humphreys 1978). In the recent catalogue of projected rotational velocities of northern O- and early B-type stars (Simón-Díaz & Herrero 2014), this star is quoted as having a low projected rotational velocity ($v \sin i$) and macroturbulent broadening component of 6 and 10 km s⁻¹, respectively.

The paper is organised as follows. Section 2 describes the observational material. Section 3 presents the results of the magnetic field detection and the analysis techniques. Section 4 details the analysis of the stellar atmosphere and the procedures employed. In Sect. 5 we discuss our results and the conclusions are drawn in Sect. 6.

2. Observations

We observed HD 54879 using the FORS 2 low-resolution spectropolarimeter (Appenzeller & Rupprecht 1992; Appenzeller et al. 1998) attached to the Cassegrain focus of the 8 m Antu telescope of the ESO Very Large Telescope of the Paranal Observatory. The observations were performed using the 2k×4k MIT CCDs (pixel size $15 \mu\text{m} \times 15 \mu\text{m}$) and a narrow slit with a width of $0.4''$, leading to a (measured) resolving power of about 1700. We also adopted the 200 kHz/low/1×1 readout mode and the GRISM 600B. Each spectrum covers the 3250 – 6215 Å spectral range which includes all Balmer lines, except $H\alpha$, and a number of He lines. The star was observed on two consecutive nights (Feb. 7 and 8, 2014) with a sequence of spectra obtained by rotating the quarter waveplate from -45° to $+45^\circ$ every second exposure (i.e., -45° , $+45^\circ$, $+45^\circ$, -45° , -45° , $+45^\circ$, etc.). The exposure times and signal-to-noise ratio (S/N) of Stokes I are listed in Table 1.

We also observed HD 54879 using the HARPSpol polarimeter (Snik et al. 2011; Piskunov et al. 2011) feeding the HARPS spectrograph (Mayor et al. 2003) attached to the ESO 3.6 m telescope in La Silla, Chile. The observations, covering the 3780 – 6910 Å wavelength range with a resolving power $R \sim 115000$, were obtained on April 23, 2014, using the circular polarisation analyser. We observed the star with a sequence of four subexposures obtained rotating the quarter-wave retarder plate by 90° after each exposure, i.e. 45° , 135° , 225° , and 315° . Each subexposure was acquired using an exposure time of 2700 seconds, leading to a Stokes I S/N per pixel of 347 at ~ 4950 Å.

¹ We consider peculiar stars those objects that show any uncommon spectral feature compared to the standard spectral type classification criteria (Walborn & Fitzpatrick 1990, 2000; Sota et al. 2011), for instance, the presence of C III $\lambda\lambda 4647 - 4650 - 4652$ Å emission lines (Walborn 1972). We do not consider $H\alpha$ as part of these classification criteria.

3. Magnetic field detection

3.1. FORS 2 observations

Because of controversies reported in the literature about magnetic field detections and measurements performed with the FORS 2 spectropolarimeter (e.g. Bagnulo et al. 2012), the data were independently reduced in Bonn and Potsdam using a different set of independent tools. The reduction and analysis performed in Bonn employed IRAF² (Tody 1993) and IDL routines based on the technique and recipes presented by Bagnulo et al. (2002, 2012), while the Potsdam reduction and analysis was based on the tools described in Hubrig et al. (2004a,b), updated to include a number of statistical tests (Schöller et al. 2014, in preparation). The details of the data reduction and analysis procedure applied in Bonn will be given in a separate work (Fossati et al., in preparation).

The longitudinal magnetic field ($\langle B_z \rangle$) was calculated using either the hydrogen lines or the full 3710 – 5870 Å spectral region. All measurements performed on the Stokes V spectrum led to detections at 6σ or more, while we consistently got non-detections from the null profile. Furthermore, Monte Carlo bootstrapping tests (Press et al. 1992; Rivinius et al. 2010; Hubrig et al. 2014c) were carried out in Potsdam. These are most often applied with the purpose of deriving robust estimates of standard errors. A total of 250000 tests were generated with the same size as the original dataset. The final $\langle B_z \rangle$ value was then determined from all these newly generated datasets. The $\langle B_z \rangle$ values and their uncertainties obtained in Bonn and Potsdam are listed in Table 1. The rather large difference between the $\langle B_z \rangle$ values obtained using the hydrogen lines and the entire spectrum might occur because, in presence of a strong magnetic field, Stokes V does not behave linearly with the derivative of Stokes I for the metallic lines; in other words, for the metallic lines the weak-field approximation, on which the method is based, does not hold anymore. A thorough discussion about this topic can be found in Landstreet et al. (2014).

3.2. HARPS observations

As was done for the FORS 2 data, the HARPS observations were reduced separately in Bonn and Potsdam, using independent routines. HARPS $\langle B_z \rangle$ results are also summarised in Table 1.

3.2.1. Bonn reduction and analysis

The reduction and analysis in Bonn was performed with the *REDUCE* package (Piskunov & Valenti 2002) and the Least-Squares Deconvolution technique (LSD; Donati et al. 1997).

The one-dimensional spectra, obtained with *REDUCE*, were combined using the “ratio” method described by Bagnulo et al. (2009). The spectra were re-normalised to the intensity of the continuum obtaining a spectrum of the Stokes I (I/I_c) and V (V/I_c), plus a spectrum of the diagnostic null profile (N - see Bagnulo et al. 2009), with the corresponding uncertainties. We then analysed the profiles of the Stokes I , V , and N parameter using LSD, which combines line profiles (assumed to be identical) centred at the position of the individual lines and scaled according to the line strength and sensitivity to a magnetic field (i.e.

² Image Reduction and Analysis Facility (IRAF – <http://iraf.noao.edu/>) is distributed by the National Optical Astronomy Observatory, which is operated by the Association of Universities for Research in Astronomy (AURA) under cooperative agreement with the National Science Foundation.

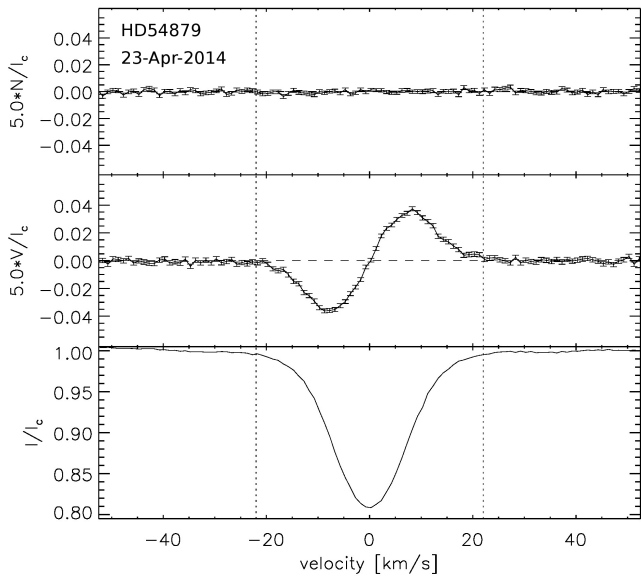


Fig. 1: LSD profiles of the Stokes I , V , and N parameter obtained for HD 54879. The error bars of the LSD profiles are shown for both Stokes V and the null parameter. The vertical dotted lines indicate the velocity range adopted for the determination of the detection probability and magnetic field value. All profiles have been shifted upwards/downwards by arbitrary values and the Stokes V and N profiles have been expanded 5 times.

line wavelength and Landé factor). We computed the LSD profiles of the Stokes I , V , and of the null profile using the methodology and the code described in Kochukhov et al. (2010). We prepared the line mask used by the LSD code adopting the stellar parameters obtained from the spectroscopic analysis (Table 2). We extracted the line parameters from the Vienna Atomic Line Database (VALD; Piskunov et al. 1995; Kupka et al. 1999; Ryabchikova et al. 1999) and tuned the given line strength to the observed Stokes I spectrum with the aid of synthetic spectra calculated with SYNTH3 (Kochukhov 2007). We used all lines stronger than 10% of the continuum, avoiding hydrogen lines, helium lines with extended wings, and lines in spectral regions affected by the presence of telluric features. The final adopted line mask contained 140 lines. We defined the magnetic field detection making use of the false alarm probability (FAP; Donati et al. 1992), considering a profile with $\text{FAP} < 10^{-5}$ as a definite detection (DD), $10^{-5} < \text{FAP} < 10^{-3}$ as a marginal detection (MD), and $\text{FAP} > 10^{-3}$ as a non-detection (ND).

Figure 1 shows the LSD profiles we obtained for HD 54879, with a S/N of the LSD Stokes V profile of 3177. The analysis of the Stokes V LSD profile led to a clear definite detection with a $\text{FAP} < 10^{-15}$, while the analysis of the LSD profile of the null parameter led to a non-detection ($\text{FAP} > 0.7$). Integrating over a range of 44 km s^{-1} (i.e. $\pm 22 \text{ km s}^{-1}$ from the line centre) we derived $\langle B_z \rangle(V) = -592 \pm 7 \text{ G}$. This result confirms the FORS 2 magnetic field detection.

Because of the high S/N of the spectra and of the strong magnetic field, the Stokes V profile presents an observable signature at the position corresponding to magnetic sensitive lines. Figure 2 shows the Stokes I , V , and null profiles for a set of strong lines of different elements. The same shape of the Stokes V profile is found for all lines. We also measured the $\langle B_z \rangle(V)$ value for some of them, obtaining results comparable to that given by the LSD profile.

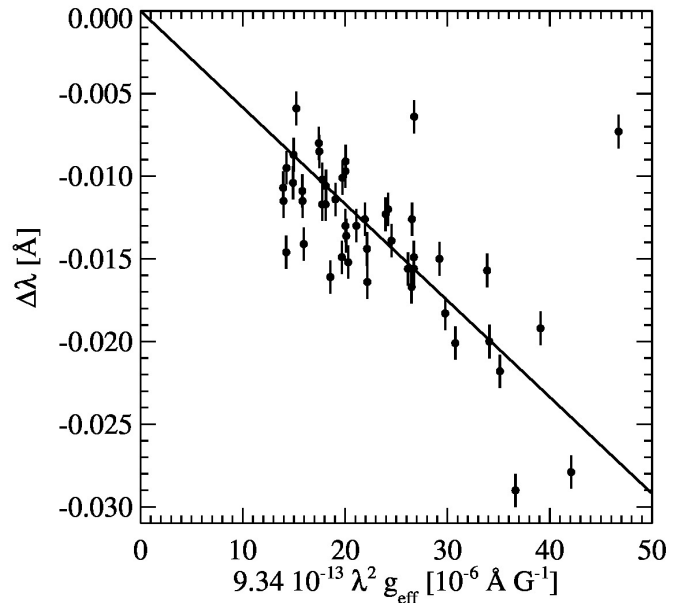


Fig. 3: Linear regression between the displacement of each line centre of gravity in the right and left circularly polarised spectra against $9.34 \cdot 10^{-13} \lambda^2 g_{\text{eff}}$ used in the moment technique (Mathys 1991).

3.2.2. Potsdam reduction and analysis

The data reduction in Potsdam was performed with the ESO/HARPS pipeline. A detailed description of the reduction and continuum normalisation is given in Hubrig et al. (2013).

A total of 49, mostly unblended, metallic lines were employed in the detection of a surface magnetic field using the moment technique (MT, Mathys 1991). This technique allows us to determine the mean longitudinal field strength and demonstrate the presence of the crossover effect and quadratic magnetic fields, and so to constrain the magnetic field topology in more detail than can be done with the LSD and Singular Value Decomposition (SVD) methods. For each line in the sample of metallic lines, the measured shifts between the line profiles in the left- and right-hand circularly polarised HARPS spectra are used in a linear regression analysis in the $\Delta\lambda$ versus $\lambda^2 g_{\text{eff}}$ diagram, following the formalism discussed by Mathys (1991, 1994) (see also Hubrig et al. 2014a, Fig. 11). The corresponding linear regression is shown in Fig. 3. The Landé factors were taken from Kurucz's list of atomic data³. For each line measured, the mean error was calculated taking into account the signal-to-noise of the spectra and the uncertainty of the wavelength calibration (Mathys 1994). We obtained a mean longitudinal magnetic field of $\langle B_z \rangle(V) = -584 \pm 15 \text{ G}$. In addition, we derived a $\langle B_z \rangle(N) = -22 \pm 10 \text{ G}$ from the spectrum of the N parameter, calculated by combining the subexposures in such a way that polarisation cancels out. Since no significant magnetic field could be detected from the null spectrum, we concluded that any noticeable spurious polarisation is absent. This is confirmed by the analysis of the LSD N profile. No crossover and mean quadratic magnetic field have been detected for this observational epoch.

In addition to the moment technique, the magnetic field was detected using the multi-line SVD technique for Stokes Profile

³ <http://kurucz.cfa.harvard.edu/atoms>

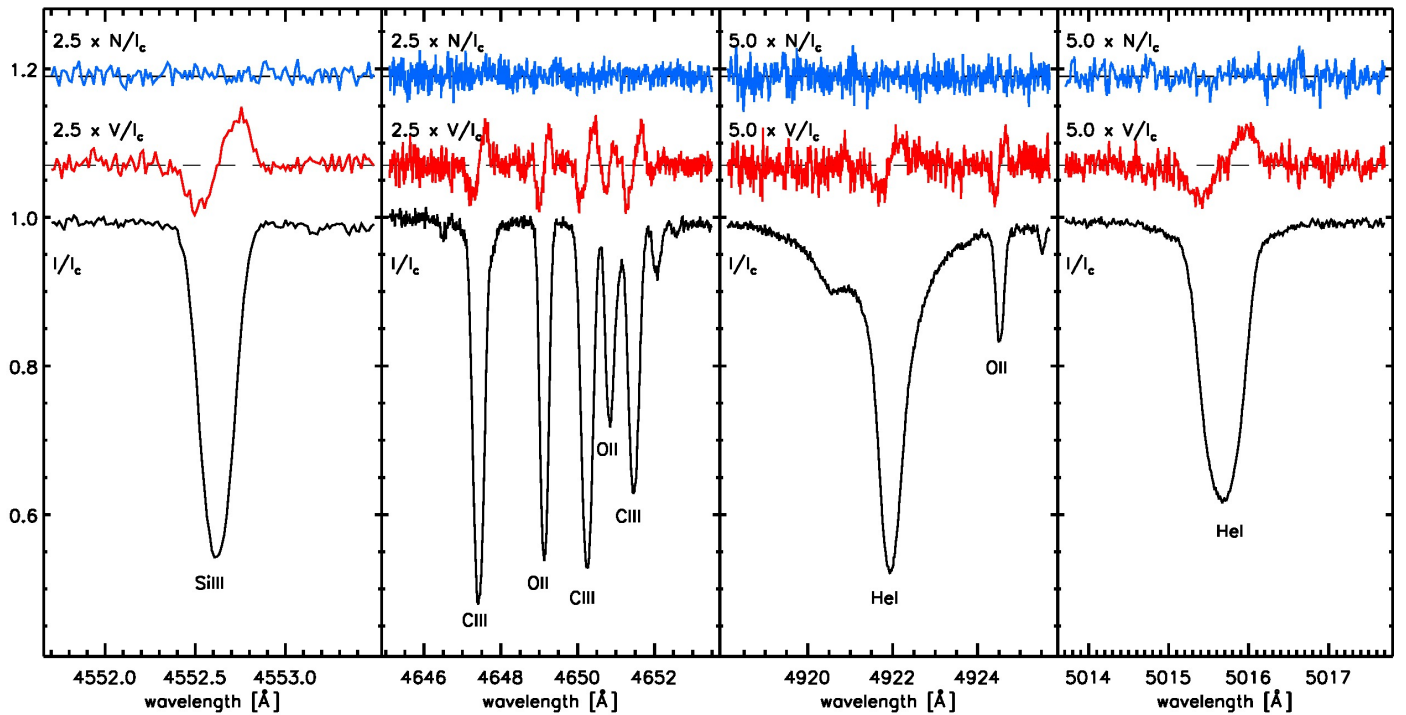


Fig. 2: The Stokes I (black bottom line), V (red middle line), and null (blue top line) profiles for a set of strong and magnetic sensitive lines. The Stokes V and null profiles have been amplified by a factor of 2.5 and shifted by an arbitrary amount.

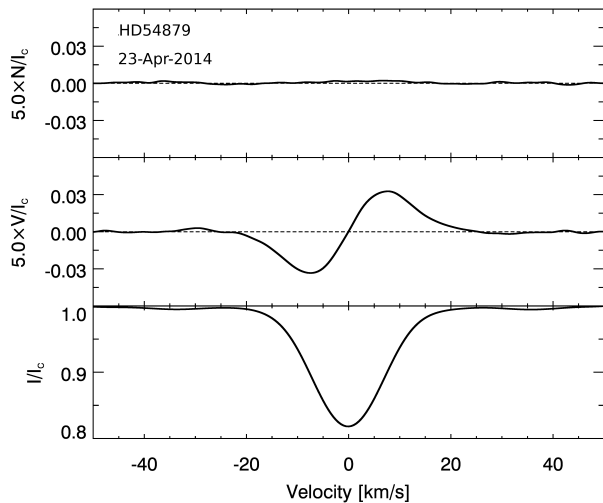


Fig. 4: SVD profile of Stokes I , V , and of the Null profile N . For display purposes the SVD profiles have been corrected for the radial velocity determined from the Stokes I profile. Like the LSD profiles, the SVD Stokes V and the N profiles have been shifted by an arbitrary amount and expanded by a factor of 5.

Reconstruction, recently introduced by Carroll et al. (2012). The results obtained with the SVD technique, using a mask of 160 lines that excludes helium and hydrogen lines, are shown in Fig. 4. As was done for the LSD analysis, the line mask was constructed using VALD. The analysis led to a definite detection with a FAP smaller than 10^{-16} . From the retrieved Stokes V profile we derived a mean longitudinal magnetic field $\langle B_z \rangle(V) = -583 \pm 9$ G.

4. Stellar parameters and abundances

The observations presented in Sect. 2 provided us with data at low and high spectral resolution, both datasets having a high S/N (> 300). We present the quantitative analysis of the datasets, aiming at 1) characterising HD 54879 through the spectra of two different instruments (i.e. FORS 2 and HARPS) and 2) exploring the impact of spectral resolution on the stellar parameters and chemical abundances.

We measured the $v \sin i$ value of nearly 130 metal transitions from the HARPS spectrum using the tool IACOB-BROAD developed by Simón-Díaz & Herrero (2014). We obtained an average $v \sin i$ value of 7 ± 2 km s $^{-1}$ and a macroturbulence of 8 ± 3 km s $^{-1}$, in agreement with Simón-Díaz & Herrero (2014). We adopted these values for our analyses.

The quantitative atmosphere analysis was performed using the stellar atmosphere code FASTWIND (Santolaya-Rey et al. 1997; Puls et al. 2005). The code enables non-LTE calculations and assumes a spherical symmetry. The velocity structure of the stellar wind is modelled with a β velocity law. Following the technique described by Castro et al. (2012) (see also Urbaneja et al. 2005 and Lefever 2007), the stellar parameters and chemical abundances were derived through automatic algorithms searching for the set of parameters that best reproduce the main transitions in the range $\sim 4000 - 4900$ Å. The automatic tools were based on a large collection of FASTWIND stellar grids (Castro et al. 2012; Simón-Díaz et al. 2011b). The chemical analysis procedure has been updated since Castro et al. (2012) by implementing an optimised genetic algorithm.

The best fitting parameters obtained from the analysis of the FORS 2 and HARPS spectra are listed in Table 2, where for comparison we added the stellar parameters of the O9.7 V standard HD 36512 (Sota et al. 2011), obtained by S. Simón-Díaz using the IACOB-GBAT code (Simón-Díaz et al. 2011b). The observed FORS 2 and HARPS spectra and the best-fit models are plotted

in Figs. 6 and 7, see also Figs. A.1 – A.3 for a detailed display of the HARPS data. The lines used in the analyses are marked. Table 2 shows the good agreement between the stellar parameters derived from the analysis of the high- and low-resolution spectra. In addition, the HD 54879 temperature and gravity values agree with those obtained for the standard star HD 36512. The analysis of the FORS 2 and HARPS spectra yield $\text{He}/\text{H} \sim 0.10 - 0.12$. The low sensitivity of the He lines to abundance variations prevents us from obtaining a more accurate value. Nevertheless, we exclude a substantial helium enhancement/depletion for this star.

The wind-strength Q-parameter⁴ estimated in HD 54879, mainly based on the Balmer lines, is substantially higher ($\log Q = -11.0$) than expected for a late-O dwarf (i.e. $\log Q = -13.46$ in HD 36512). To further investigate this difference, Fig. 8 compares high-resolution spectra of HD 54879 and HD 36512. Both spectra were taken with the same instrument as part of the IACOB project (see Sect. 5.3). Convoluting the spectrum of HD 54879 to match the rotation and macroturbulence velocities of HD 36512 reveals a remarkable similarity between the spectra of the two stars. However, the transitions formed in the outer parts of the atmosphere show noticeable differences, especially $\text{H}\alpha$. It is unlikely that an exceptionally strong stellar wind is at the origin of the $\text{H}\alpha$ emission, which instead most probably originates from circumstellar material in the magnetosphere (see Sect. 5.1), as already reported in other stars (e.g. Walborn 1980; Grunhut et al. 2009). We therefore re-calculated the stellar parameters without considering the lines most sensitive to the external atmospheric layers. The new parameters obtained in this way are identical to the original values.

We used BONNSAI⁵ (Schneider et al. 2014) to determine the current mass, radius, and age of HD 54879. BONNSAI computes the full posterior probability distributions of stellar parameters using Bayes' theorem. The code simultaneously matches the derived effective temperature, surface gravity, and projected rotational velocity of HD 54879 to the Milky Way single-star models of Brott et al. (2011). We assumed a Salpeter initial mass function (Salpeter 1955) as initial mass prior and uniform priors for the age and initial rotational velocity. The stellar rotation axes are randomly oriented in space.

The fundamental parameters derived by BONNSAI are listed in Table 3 together with the spectroscopic values. The spectroscopic luminosity (L), current mass (M), and radius (R) were calculated taking a distance of 1.32 kpc (Humphreys 1978), the spectral energy distribution provided by FASTWIND, the extinction laws of Fitzpatrick & Massa (2007), and HD 54879 optical and 2MASS photometry. Figure 5 shows the comparison of the FASTWIND synthetic fluxes, calculated by adopting the fundamental parameters derived for HD 54879 with the available ultraviolet (UV, Thompson et al. 1978), optical (Mermilliod & Mermilliod 1994), and infrared (IR, Cutri et al. 2003; Cutri et al. 2012) photometry. The discrepancy between the synthetic flux and WISE photometry is a known issue (Fossati et al. 2014). WISE magnitudes were not used in the spectroscopic parameters reported in Table 3. The match between BONNSAI and the spectroscopic values highlights the consistency between the stellar tracks prediction, distance, and photometry of HD 54879. The fractional main-sequence age derived from the Brott et al. (2011) evolutionary tracks is 0.46. The age derived with BONNSAI (see

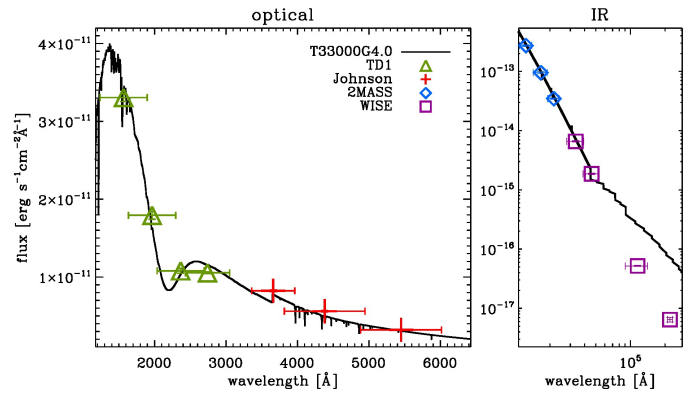


Fig. 5: Comparison between FASTWIND (full black line) synthetic flux and TD1 (green triangles), Johnson (red pluses), 2MASS (blue diamonds), and WISE (purple squares) photometry converted into physical units. The UV and optical spectral regions are shown in the left panel and the IR band in the right panel.

Table 3: HD 54879 theoretical (BONNSAI) and spectroscopic (Spec.) stellar parameters.

HD 54879	BONNSAI	Spec.
$\log L/L_{\odot}$	$4.7^{+0.2}_{-0.2}$	$4.7^{+0.3}_{-0.2}$
R/R_{\odot}	$6.7^{+1.0}_{-0.9}$	$6.8^{+2.3}_{-1.6}$
M/M_{\odot}	$18.6^{+2.0}_{-1.6}$	$16.9^{+1.1}_{-1.0}$
Age (Myr)	$4.0^{+0.8}_{-1.2}$	

Table 3) agrees with that of the CMa OB1 association of which the star is a probable member (3 Myr, Clariá 1974).

The obtained non-LTE chemical abundances are listed in Table 2, together with the solar abundances by Asplund et al. (2009) and the present-day massive star abundances in the solar neighbourhood by Nieva & Przybilla (2012). The abundance values derived from the HARPS and FORS 2 spectra agree within the errors. The low resolution hampers a precise abundance determination of some chemical elements. For instance, the measurement of the nitrogen abundance is based on weak lines (e.g. $\text{N II } \lambda \sim 3995 \text{ \AA}$) that are clearly visible in the HARPS spectrum (Fig. 7), but blurred in the continuum at the low resolution of FORS 2 (Fig. 6). Oxygen presents strong lines that are clearly visible, hence measurable, even at low resolution.

5. Discussion

5.1. General considerations about the detected magnetic field

The $\langle B_z \rangle$ values independently obtained in Bonn and Potsdam agree within the uncertainties. The FORS 2 results from Bonn indicate slightly larger fields than those from Potsdam. The magnetic fields derived from HARPS data in Bonn and Potsdam are practically identical. The LSD, SVD, and MT, on average, provide $\langle B_z \rangle(V) = -586 \pm 5 \text{ G}$.

With the few available magnetic field measurements it is not possible to perform a meaningful modelling of the magnetic field topology and strength, particularly with measurements conducted with completely different instruments and techniques (Landstreet et al. 2014). Nevertheless, from the maxi-

⁴ The Q-parameter (Puls et al. 1996; Kudritzki & Puls 2000) is a measurement of the stellar wind strength defined as $Q = \dot{M} / (R_* v_{\infty})^{1.5}$, where \dot{M} is the mass-loss rate, R_* the stellar radius, and v_{∞} the terminal wind velocity.

⁵ The BONNSAI web-service is available at <http://www.astro.uni-bonn.de/stars/bonnsai>

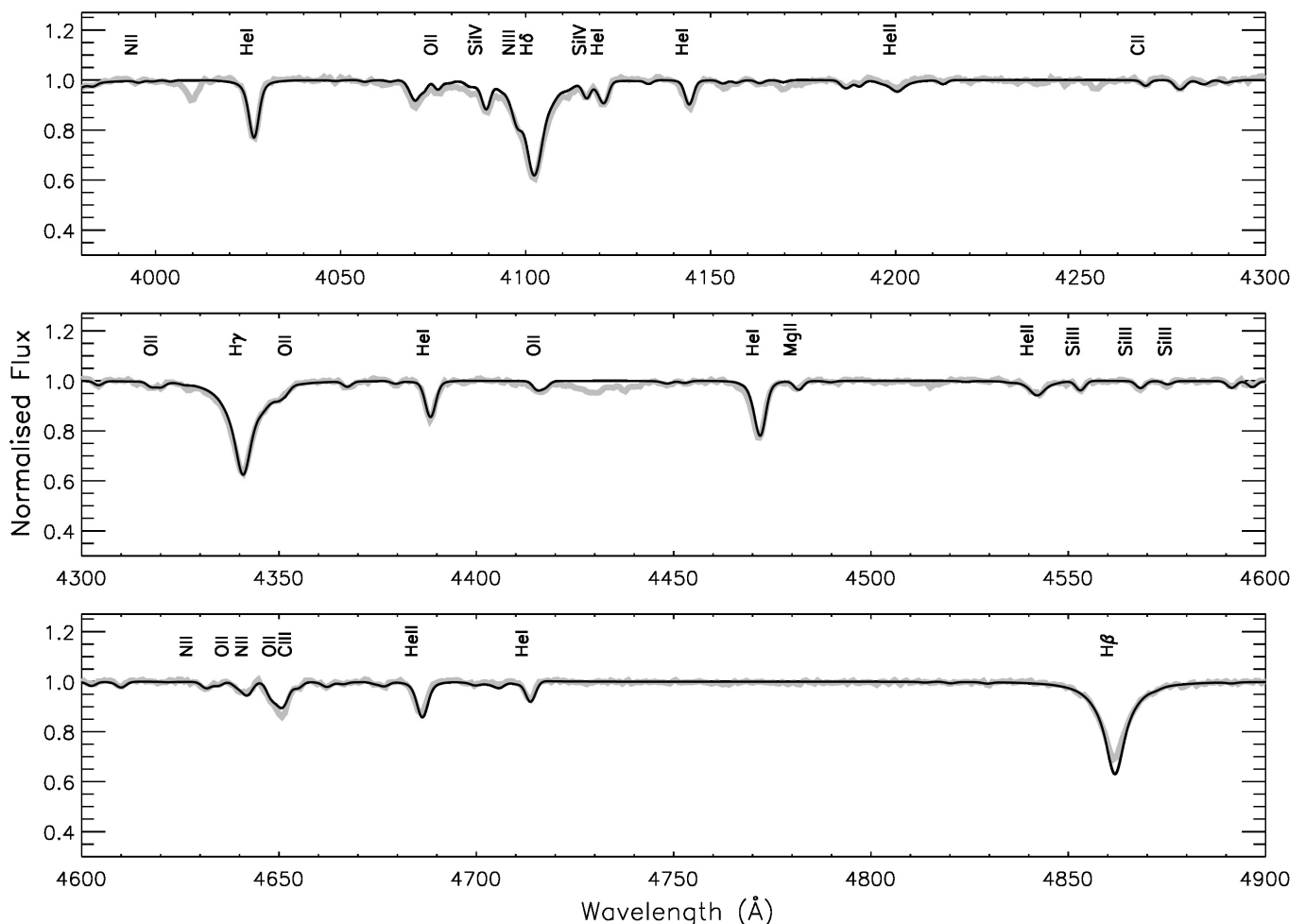


Fig. 6: Normalised FORS 2 optical spectrum (grey) and the best-fit FASTWIND stellar model (black). The lines included in the analysis are marked.

imum recorded $|\langle B_z \rangle|$ value it is possible to derive the expected minimum dipolar magnetic field strength (B_d ; e.g. Eq 7 of Aurière et al. 2007). From both FORS 2 and HARPS measurements we derived a maximum $|\langle B_z \rangle|$ of the order of 600 G, implying $B_d \gtrsim 2.0$ kG. Despite the strong magnetic field, we have found no sign of photospheric line profile variations (Sect. 5.3).

The dipolar field strength of HD 54879 places this star at the same magnetic strength level as the fast-rotating secondary of Plaskett’s star (Grunhut et al. 2013) and ALS 15218 (Nazé et al. 2012). Radial velocity variations have been reported for ALS 15218 (Combi et al. 2011), so it may also be part of a binary system. In contrast, HD 54879 is apparently a slowly rotating single star, though we cannot rule out a pole-on view, and is probably the strongest magnetic non-peculiar and single O-type star detected so far.

In the context of the classification of magnetospheres of massive stars presented by Petit et al. (2013) and assuming a minimum dipolar magnetic field strength of 2.0 kG and an equator-on view, we obtained a lower limit on the Alfvén radius of about 5 stellar radii and an upper limit on the Keplerian corotation radius of about 20 stellar radii. For the calculation of the Alfvén and Keplerian corotation radius we adopted the stellar parameters obtained from BONNSAI, a terminal velocity of 1700 km s^{-1} (Kudritzki & Puls 2000) and the mass-loss rate obtained from

the relation given by Vink et al. (2000). The derived values indicate that the star has a dynamical magnetosphere, but one has to keep in mind that the Alfvén radius is a lower limit and the Keplerian corotation radius is an upper limit, hence the star could have a centrifugal magnetosphere (Townsend & Owocki 2005; Maheswaran & Cassinelli 2009; Petit et al. 2013). Moreover, HD 54879 is in the weak wind regime of late-O dwarfs as discussed by Martins et al. (2005). In this regime, the mass-loss rates might be up to a factor of hundred lower than expected from theory (Puls et al. 2008), whereas the hydrodynamically measured rate of the O9.5 dwarf ζ Oph (Gvaramadze et al. 2012) is found to be only a factor of six below that predicted by Vink et al. (2000) (see also Huenemoerder et al. 2012). A smaller mass-loss rate would lead to a larger Alfvén radius, placing the star closer to the region covered by stars with a centrifugal magnetosphere; this region could then be reached with a slightly shorter rotational period (i.e., a non-orthogonal inclination angle).

The mass-loss rate obtained for HD 54879, assuming a line-driven stellar wind as the unique cause of $H\alpha$ emission, is too large according to its spectral type and previous studies of late O-type dwarfs (Fig. 8, see also Simón-Díaz et al. 2006; Najarro et al. 2011; Martins et al. 2012b). HD 54879 fits in the Oe-star category, as defined by Conti & Leep (1974) (see also Negueruela et al. 2004). The classical Be scenario suggests a circumstel-

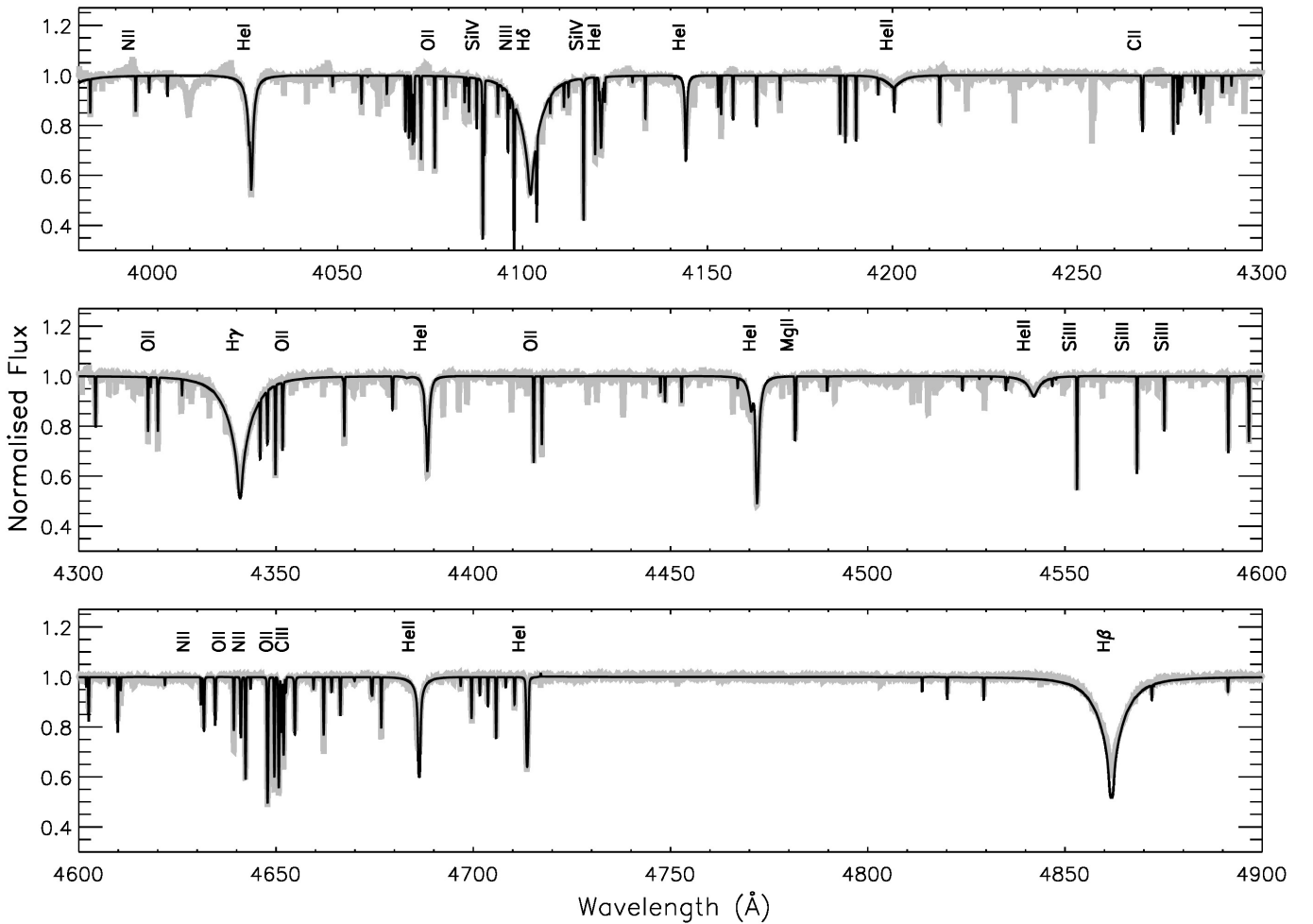


Fig. 7: Same as Fig. 6 but for the HARPS normalised spectrum. Only the main transitions for the spectral and chemical analysis have been modelled (Castro et al. 2012).

lar disk produced by a rapidly rotating star (Porter & Rivinius 2003). In the case of HD 54879, a centrifugal magnetosphere supported by the strong magnetic field could be responsible for the circumstellar H α emission.

The low $v \sin i$ observed in HD 54879 could also be a consequence of the strong magnetic field (Deutsch 1958; Sundqvist et al. 2013). Magnetic braking can remove angular momentum when the stellar outflow remains coupled to the magnetic field as it leaves the star (e.g. Mestel & Spruit 1987; Ud-Doula et al. 2009; Petit et al. 2013).

5.2. General considerations about the stellar atmosphere analysis

The analysis of the stellar parameters places HD 54879 on the main-sequence phase with an age of $4.0^{+0.8}_{-1.2}$ Myr, according to the Brott et al. (2011) evolutionary tracks. The chemical abundances, inferred from the HARPS data, are slightly lower than the solar values (Asplund et al. 2009) and the cosmic abundance standard obtained by Nieva & Przybilla (2012), though still compatible within the uncertainties. Neither helium nor the other chemical elements analysed show any noteworthy peculiarity.

The differences between spectroscopic and evolutionary masses have been a source of conflict (Herrero et al. 1992), al-

though improvements in both fields have reduced the discrepancies (Mokiem et al. 2007; Rivero González et al. 2012; Bouret et al. 2013). HD 54879 shows a difference in $\log M_{\text{spec}}/M_{\text{evol}} = -0.04 \pm 0.05$ dex. Although this is only one star, the result supports the reliability of our routines, analysis techniques, and stellar models. Nevertheless, a large sample of stars is required to determine whether the systematic $\log M_{\text{spec}}/M_{\text{evol}} = -0.06$ dex offset reported by U et al. (2009) (see also Fig. 9 in Castro et al. 2012) still persists when taking into account the latest state-of-the-art developments in the stellar theory and analysis techniques (see also Markova & Puls 2014).

We would like to note the good agreement between the high and low spectral resolution stellar atmosphere analyses. This test provides additional confidence in previous studies carried out using low spectral resolution data (e.g. Evans et al. 2007; U et al. 2009; Castro et al. 2012), with a note of caution concerning the chemical analysis described in Sect. 4.

5.3. Radial velocities and line profile variations

The strong magnetic field detected in HD 54879 could lead to line profile variations (see e.g. Piskunov & Kochukhov 2002; Kochukhov & Sudnik 2013). To check for spectral variability we have complemented our HARPS observations with high-

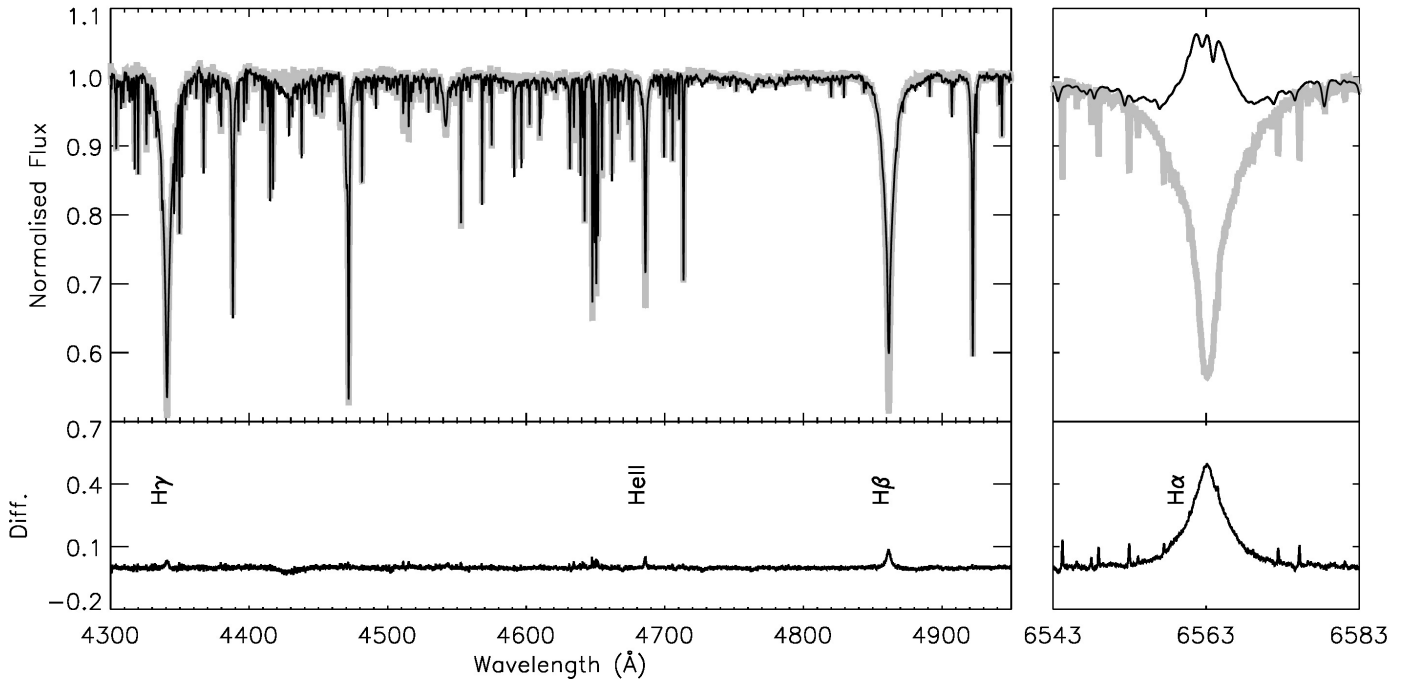


Fig. 8: Top panels: optical spectra of HD 54879 taken on Jan. 15, 2011 (black), and the O9.7 V standard HD 36512 (grey). Bottom panels: difference between the two stars, after convolving HD 54879 to match the broadening of HD 36512. The lines showing the most substantial differences are highlighted. The mismatch at 4428 Å is the result of a diffuse interstellar band.

resolution ($R \sim 50000$) spectra from the IACOB (Simón-Díaz et al. 2011a; Simón-Díaz & Herrero 2014; Simón-Díaz et al. 2015) and OWN (Barbá et al. 2010) surveys. This resulted in eight additional spectra (three obtained with FIES@NOT2.5 and five with FEROS@ESO2.2). All the collected high-resolution spectra were obtained between 2009 and 2014. The observing dates and radial velocity measurements, derived from the average of the individual lines marked in Fig. 7, are summarised in Table 4. Boyajian et al. (2007) calculated for HD 54879 a constant radial velocity of $35.4 \pm 1.4 \text{ km s}^{-1}$. The authors also mentioned a previous radial velocity measurement by Neubauer (1943) of $15.6 \pm 1.4 \text{ km s}^{-1}$. These results might suggest that the star is a member of a long-period (i.e. tens of years) binary, although no companion was found in interferometry studies by Mason et al. (1998) and Sana et al. (2014). Given the negligible radial velocity variation measured from the spectra listed in Table 4, and a lack of companions in high angular resolution studies, we assume the single-star scenario for HD 54879.

By combining the stellar radius (Table 3) and the $v \sin i$ value obtained for HD 54879, we derived a maximum rotation period of 43 days. Given the short period and time sampling of our high-resolution spectra, line profile variations due to spots should be clearly detectable. The left panel of Fig. 9 reveals instead that the shape of the photospheric lines does not vary with time. A pole-on view of HD 54879 could explain the lack of line profile variations, but the magnetic field variations discard this hypothesis. In contrast, the $H\alpha$ line (right panel of Fig. 9) presents evident variations. The line profiles shown in Fig. 9 hint to a stable $H\alpha$ emission with two outbursts detected on Feb. 13, 2011, and Apr. 23, 2014. The FEROS spectrum obtained on Feb. 13, 2011, shows some line variations, but these are most likely due to problems in the continuum normalisation. Despite this last issue, we

Table 4: HD 54879 radial velocities between 2009 and 2014 obtained with three different spectrographs (see Sect. 5.3).

ID	Date	HJD- 2450000	Vrad. (km s^{-1})
HARPS	23-Apr-2014	6770.4652	29.5 ± 1.0
FIES	16-Feb-2013	6339.5189	29.0 ± 3.0
FIES	26-Dec-2012	6287.6420	29.0 ± 1.0
FEROS	19-May-2012	6067.4686	29.0 ± 2.0
FEROS	17-May-2011	5699.4522	29.0 ± 2.0
FEROS	22-Mar-2011	5642.5125	30.0 ± 2.0
FEROS	13-Feb-2011	5605.6578	30.5 ± 3.0
FIES	15-Jan-2011	5576.5463	28.5 ± 2.0
FEROS	01-May-2009	4953.4889	29.0 ± 2.0

retained the Feb. 13, 2011, spectrum in this study because of its relevance for the $H\alpha$ line profile variations.

5.4. Magnetic field–peculiarities links

Figure 10 shows the position of the known magnetic chemically peculiar B-type stars (Bp stars) in the HRD. Chemical peculiarities in these objects are closely linked to the magnetic field (e.g. Berger 1956; Pedersen & Thomsen 1977; Borra & Landstreet 1979; Kochukhov et al. 2011; Bailey et al. 2014) and arise as a result of diffusion processes (i.e. that depend on the balance between gravitational settling and radiative levitation; Michaud 1970). The magnetic B-type stars falling in the same region of the HRD as the Bp stars are also expected to present chemical pe-

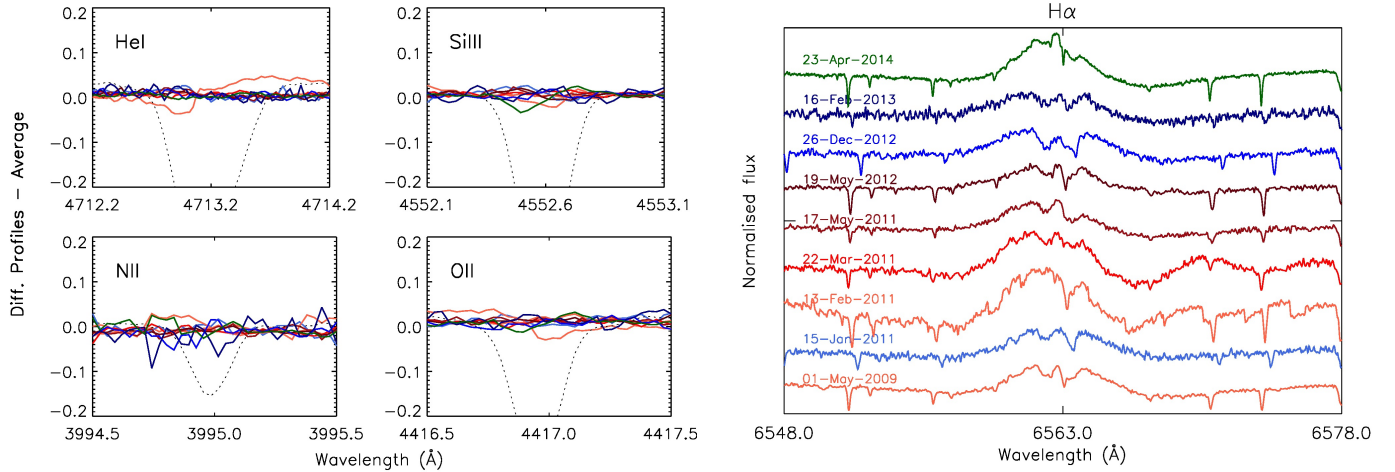


Fig. 9: Left panels: difference for four lines between the average profile and all the observations presented in Table 4. The colour code is indicated in the right panel. The average profiles are overplotted (black dotted line). Right panel: Time series of H α profile between 2009 and 2014. The narrow absorption transitions correspond to telluric features.

culiarities (see e.g. Alecian et al. 2014), but a detailed abundance analysis has not been performed yet for all of them. The stellar wind sets the upper limit in temperature and mass at which a B-type star may develop surface chemical peculiarities as a result of diffusion and, in theory, a plot such as Fig. 10 would allow these important boundaries to be determined. In practice, this is complicated by the fact that the wind is line-driven and therefore the surface abundances (Krtićka 2014), as well as the magnetic field, control the wind strength. As stars may have different magnetic field (strengths and topologies) and surface abundances (still to be determined in several cases), it is not yet possible to firmly constrain the upper temperature and mass boundary of diffusion in magnetic stars. Still, Fig. 10 suggests a boundary at about 10 M_{\odot} and 25000 K.

HD 54879 seems to show remarkable differences compared to the other known magnetic O-type stars. The star does not present the spectral features typical of Of?p stars and, in addition, it does not present the peculiarity and variability displayed by HD 37022 (θ^1 Ori C) (Stahl et al. 1993; Walborn & Nichols 1994). The other magnetic O-type stars also present peculiarities of some sort and spectral variability: Plaskett’s star appears to be the mass gainer in the HD 47129 binary system (Grunhut et al. 2013), and HD 37742 (ζ Ori Aa) is an evolved rapidly rotating O-type star with a very weak magnetic field (anomalous for magnetic massive stars; Bouret et al. 2008). A wide variety of spectral variability for the apparently normal stars ALS 15128 (Nazé et al. 2012; Combi et al. 2011) and HD 57682 (Grunhut et al. 2009, 2012) has also been reported. HD 54879 instead does not show any spectral peculiarity or line profile variability in the photospheric lines and appears to be the only known magnetic single O dwarf to date with an apparently normal and stable photospheric spectrum. Walborn et al. (2010) (see also Walborn 1972) classified the Of?p stars mainly according to the presence of C III $\lambda\lambda 4647 - 4650 - 4652$ Å emission lines. It could be that HD 54879 is simply not hot and luminous enough to display the morphological features of the stars belonging to the Of?p class.

5.5. Similarities with τ Sco

The optical spectrum of HD 54879 resembles that of τ Sco. Both stars have a low $v \sin i$ and a similar effective temperature and

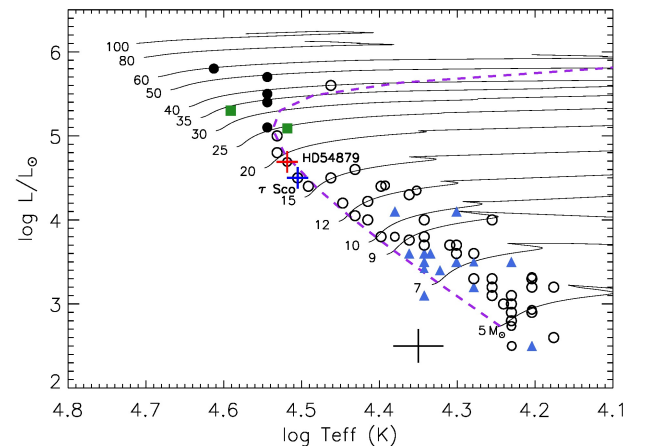


Fig. 10: Position in the Hertzsprung–Russell diagram of OB-stars with a confirmed magnetic field detection (Briquet et al. 2013; Petit et al. 2013; Alecian et al. 2014; Fossati et al. 2014, 2015; Neiner et al. 2014) and Brott et al. (2011) evolutionary tracks. Stars with an Of?p spectral classification are highlighted with black dots. Other peculiar O-stars are indicated by green squares. HD 54879 is labelled and shown with an additional red cross. Blue triangles indicate B stars classified as peculiar in the works cited. An isochrone close to the age of HD 54879, 4.0 Myr, is plotted (purple dashed line). The average uncertainties in effective temperature and luminosity are illustrated by the black cross in the bottom part of the plot. The magnetic star in the Trifid nebula detected by Hubrig et al. (2014b) is not included here because of the difficulties in establishing its properties. τ Sco has also been labelled and marked (blue cross).

surface gravity (Nieva & Przybilla 2012), see Fig. 10. However, HD 54879 does not share other peculiarities reported for τ Sco, particularly the relatively high nitrogen-to-carbon ratio presented by τ Sco is not found in HD 54879. Nieva & Przybilla (2014) claim that τ Sco is a blue straggler that has been rejuvenated either by a merger or by mass accretion in a binary system. The agreement between the age derived from BONSAI and that of

the CMa OB1 association suggests that HD 54879 is not a blue straggler (i.e. it has not been rejuvenated). There might also be a difference in the magnetic field topology, but more polarimetric observations of HD 54879 are required to conclude anything on this.

Petit et al. (2011) presented two stars that appear to be analogues to τ Sco based on their T_{eff} and $\log g$ values, the detection of magnetic fields, and UV spectral characteristics. There are no UV data available for HD 54879.

6. Conclusions

We report the first measurement of a magnetic field in HD 54879, a presumably single O9.7 V star with a low projected rotational velocity, observed in the context of the BOB collaboration. Based on HARPS and FORS 2 spectropolarimetric data we characterised the stellar atmosphere of HD 54879 and unambiguously detected a strong magnetic field using independent techniques. The magnetic field measurements were carried out in two independent ways, and reached consistent values. We derived a lower limit on the polar magnetic field of ~ 2.0 kG.

We analysed the optical spectra of HD 54879 using FASTWIND grids and automatic routines. Both FORS 2 and HARPS datasets yield almost identical effective temperature and surface gravity. The same is true for the chemical abundances. The chemical composition is systematically lower than the solar one (Asplund et al. 2009) and lower than the cosmic abundance standard from Nieva & Przybilla (2012), but compatible with both within the uncertainties; neither obvious enhancements nor depletions were found. The match between low and high spectral resolution analyses supports the robustness of our results and lends confidence to previous quantitative analyses based on low spectral resolution data.

The mass-loss rate derived based on the $H\alpha$ emission is unexpectedly large for an O9.7 V star. A comparison with a standard star of a similar spectral type (HD 36512), and with previous works on O9-B0 dwarfs confirmed this, rejecting $H\alpha$ as a reliable mass-loss rate indicator for HD 54879. Our analysis suggests that circumstellar material is a more plausible explanation for the $H\alpha$ emission. The measurable differences in the Balmer lines and $\text{He II } \lambda 4686 \text{ \AA}$ are also ascribed to circumstellar material.

We explored line profile variability using high spectral resolution data from the IACOB and OWN surveys. We checked for changes in nine spectra covering six years. The optical photospheric transitions remain unchanged. The $H\alpha$ emission displays a fairly stable shape with an enhanced emission in the line core in 2011 and 2014. This could be an indication for periodical outburst events, but more data are needed to establish this.

The optical spectrum resembles that of τ Sco, but unlike τ Sco itself, HD 54879 presents surface abundances compatible with the solar and the standard cosmic abundances. In addition, the age of HD 54879 matches the age of the CMa OB1 association, to which this star probably belongs. These considerations make the blue straggler hypothesis unlikely and suggest that the magnetic field was not generated by a merger of two main-sequence stars.

HD 54879 is, so far, the strongest magnetic single O-type star detected with a stable and normal optical spectrum, with the exception of the lines partly formed in the magnetosphere. We have not detected any distinctive spectral feature observed in other magnetic O-type stars (i.e. Of?p objects). Nonetheless, it may be a consequence of the star's lower temperature and luminosity compared to the known Of?p stars.

HD 54879 is certainly an interesting object to follow up. The strong magnetic field makes this star a good candidate for exploring the apparent ordered magnetic geometry and $H\alpha$ variability. The apparent link between $H\alpha$ emission, not expected according to its spectral type, and a magnetosphere offers a criterion for selecting magnetic candidates.

Acknowledgements. The authors thank the referee for useful comments and helpful suggestions that improved this manuscript. LF acknowledges financial support from the Alexander von Humboldt Foundation. SS-D and AH thank funding from the Spanish Government Ministerio de Economía y Competitividad (MINECO) through grants AYA2010-21697-C05-04, AYA2012-39364-C02-01 and Severo Ochoa SEV-2011-0187, and the Canary Islands Government under grant PID2010119. TM acknowledges financial support from Belspo for contract PRODEX GAIA-DPAC. FRNS acknowledges the fellowship awarded by the Bonn-Cologne Graduate School of Physics and Astronomy. NL and AR thank the DFG (Germany) and CONICYT (Chile) for the International Collaboration Grant DFG-06. The authors thank Andreas Irrgang for helping in the FEROS data reduction.

References

- Alecian, E., Kochukhov, O., Petit, V., et al. 2014, *A&A*, 567, A28
 Appenzeller, I., Fricke, K., Fürtig, W., et al. 1998, *The Messenger*, 94, 1
 Appenzeller, I. & Rupprecht, G. 1992, *The Messenger*, 67, 18
 Asplund, M., Grevesse, N., Sauval, A. J., & Scott, P. 2009, *ARA&A*, 47, 481
 Aurière, M., Wade, G. A., Silvester, J., et al. 2007, *A&A*, 475, 1053
 Bagnulo, S., Landolfi, M., Landstreet, J. D., et al. 2009, *PASP*, 121, 993
 Bagnulo, S., Landstreet, J. D., Fossati, L., & Kochukhov, O. 2012, *A&A*, 538, A129
 Bagnulo, S., Szeifert, T., Wade, G. A., Landstreet, J. D., & Mathys, G. 2002, *A&A*, 389, 191
 Bailey, J. D., Landstreet, J. D., & Bagnulo, S. 2014, *A&A*, 561, A147
 Barbá, R. H., Gamen, R., Arias, J. I., et al. 2010, in *Revista Mexicana de Astronomía y Astrofísica Conference Series*, Vol. 38, 30–32
 Berger, J. 1956, *Contr. Inst. Ap. Paris*, Ser. A, 217
 Borra, E. F. & Landstreet, J. D. 1979, *ApJ*, 228, 809
 Borra, E. F. & Landstreet, J. D. 1980, *ApJS*, 42, 421
 Bouret, J.-C., Donati, J.-F., Martins, F., et al. 2008, *MNRAS*, 389, 75
 Bouret, J.-C., Lanz, T., Martins, F., et al. 2013, *A&A*, 555, A1
 Boyajian, T. S., Gies, D. R., Baines, E. K., et al. 2007, *PASP*, 119, 742
 Briquet, M., Neiner, C., Aerts, C., et al. 2012, *MNRAS*, 427, 483
 Briquet, M., Neiner, C., Leroy, B., & Pápics, P. I. 2013, *A&A*, 557, L16
 Brott, I., de Mink, S. E., Cantiello, M., et al. 2011, *A&A*, 530, A115+
 Carroll, T. A., Strassmeier, K. G., Rice, J. B., & Küstler, A. 2012, *A&A*, 548, A95
 Castro, N., Urbaneja, M. A., Herrero, A., et al. 2012, *A&A*, 542, A79
 Clariá, J. J. 1974, *A&A*, 37, 229
 Combi, J. A., Albacete-Colombo, J. F., Luque Escamilla, P. L., et al. 2011, *Bulletin de la Societe Royale des Sciences de Liege*, 80, 644
 Conti, P. S. & Leep, E. M. 1974, *ApJ*, 193, 113
 Cutri, R. M. & et al. 2012, *VizieR Online Data Catalog*, 2311, 0
 Cutri, R. M., Skrutskie, M. F., van Dyk, S., et al. 2003, *VizieR Online Data Catalog*, 2246, 0
 Deutsch, A. J. 1958, *Handbuch der Physik*, 51, 689
 Donati, J.-F., Babel, J., Harries, T. J., et al. 2002, *MNRAS*, 333, 55
 Donati, J.-F., Howarth, I. D., Bouret, J.-C., et al. 2006, *MNRAS*, 365, L6
 Donati, J.-F. & Landstreet, J. D. 2009, *ARA&A*, 47, 333
 Donati, J.-F., Semel, M., Carter, B. D., Rees, D. E., & Collier Cameron, A. 1997, *MNRAS*, 291, 658
 Donati, J.-F., Semel, M., & Rees, D. E. 1992, *A&A*, 265, 669
 Evans, C. J., Bresolin, F., Urbaneja, M. A., et al. 2007, *ApJ*, 659, 1198
 Ferrario, L., Pringle, J. E., Tout, C. A., & Wickramasinghe, D. T. 2009, *MNRAS*, 400, L71
 Fitzpatrick, E. L. & Massa, D. 2007, *ApJ*, 663, 320
 Fossati, L., Castro, N., Morel, T., et al. 2015, *A&A*, 574, A20
 Fossati, L., Zwintz, K., Castro, N., et al. 2014, *A&A*, 562, A143
 Grunhut, J. H., Wade, G. A., Leutenegger, M., et al. 2013, *MNRAS*, 428, 1686
 Grunhut, J. H., Wade, G. A., Marcolino, W. L. F., et al. 2009, *MNRAS*, 400, L94
 Grunhut, J. H., Wade, G. A., Sundqvist, J. O., et al. 2012, *MNRAS*, 426, 2208
 Gvarnadze, V. V., Langer, N., & Mackey, J. 2012, *MNRAS*, 427, L50
 Herrero, A., Kudritzki, R. P., Vilchez, J. M., et al. 1992, *A&A*, 261, 209
 Hubrig, S., Castelli, F., González, J. F., et al. 2014a, *MNRAS*, 442, 3604
 Hubrig, S., Fossati, L., Carroll, T. A., et al. 2014b, *A&A*, 564, L10
 Hubrig, S., Ilyin, I., Schöller, M., & Lo Curto, G. 2013, *Astronomische Nachrichten*, 334, 1093
 Hubrig, S., Kurtz, D. W., Bagnulo, S., et al. 2004a, *A&A*, 415, 661

- Hubrig, S., North, P., & Schöller, M. 2007, *Astronomische Nachrichten*, 328, 475
- Hubrig, S., Schöller, M., Fossati, L., et al. 2015, *A&A*, 578, L3
- Hubrig, S., Schöller, M., Kharchenko, N. V., et al. 2011, *A&A*, 528, A151
- Hubrig, S., Schöller, M., & Kholtygin, A. F. 2014c, *MNRAS*, 440, 1779
- Hubrig, S., Schöller, M., Schnerr, R. S., et al. 2008, *A&A*, 490, 793
- Hubrig, S., Szeifert, T., Schöller, M., Mathys, G., & Kurtz, D. W. 2004b, *A&A*, 415, 685
- Huenemoerder, D. P., Oskinova, L. M., Ignace, R., et al. 2012, *ApJ*, 756, L34
- Humphreys, R. M. 1978, *ApJS*, 38, 309
- Kochukhov, O. & Bagnulo, S. 2006, *A&A*, 450, 763
- Kochukhov, O., Lundin, A., Romanyuk, I., & Kudryavtsev, D. 2011, *ApJ*, 726, 24
- Kochukhov, O., Makaganiuk, V., & Piskunov, N. 2010, *A&A*, 524, A5
- Kochukhov, O. & Sudnik, N. 2013, *A&A*, 554, A93
- Kochukhov, O. P. 2007, in *Physics of Magnetic Stars*, ed. I. I. Romanyuk, D. O. Kudryavtsev, O. M. Neizvestnaya, & V. M. Shapoval, 109–118
- Krtićka, J. 2014, *A&A*, 564, A70
- Kudritzki, R.-P. & Puls, J. 2000, *ARA&A*, 38, 613
- Kupka, F., Piskunov, N., Ryabchikova, T. A., Stempels, H. C., & Weiss, W. W. 1999, *A&AS*, 138, 119
- Landstreet, J. D. 1992, *A&A Rev.*, 4, 35
- Landstreet, J. D., Bagnulo, S., Andretta, V., et al. 2007, *A&A*, 470, 685
- Landstreet, J. D., Bagnulo, S., & Fossati, L. 2014, *A&A*, 572, A113
- Landstreet, J. D., Silaj, J., Andretta, V., et al. 2008, *A&A*, 481, 465
- Langer, N. 2012, *ARA&A*, 50, 107
- Langer, N. 2014, in *IAU Symposium*, Vol. 302, *IAU Symposium*, 1–9
- Lefever, K. 2007, PhD thesis, K. U. Leuven
- Maeder, A. & Meynet, G. 2000, *ARA&A*, 38, 143
- Maheswaran, M. & Cassinelli, J. P. 2009, *MNRAS*, 394, 415
- Markova, N. & Puls, J. 2014, *ArXiv e-prints*: 1409.7784
- Martins, F., Donati, J.-F., Marcolino, W. L. F., et al. 2010, *MNRAS*, 407, 1423
- Martins, F., Escolano, C., Wade, G. A., et al. 2012a, *A&A*, 538, A29
- Martins, F., Mahy, L., Hillier, D. J., & Rauw, G. 2012b, *A&A*, 538, A39
- Martins, F., Schaerer, D., Hillier, D. J., et al. 2005, *A&A*, 441, 735
- Mason, B. D., Gies, D. R., Hartkopf, W. I., et al. 1998, *AJ*, 115, 821
- Mathys, G. 1991, *A&AS*, 89, 121
- Mathys, G. 1994, *A&AS*, 108, 547
- Mayor, M., Pepe, F., Queloz, D., et al. 2003, *The Messenger*, 114, 20
- Mermilliod, J.-C. & Mermilliod, M. 1994, *Catalogue of Mean UBV Data on Stars*
- Mestel, L. & Spruit, H. C. 1987, *MNRAS*, 226, 57
- Michaud, G. 1970, *ApJ*, 160, 641
- Mokiem, M. R., de Koter, A., Evans, C. J., et al. 2007, *A&A*, 465, 1003
- Morel, T., Castro, N., Fossati, L., et al. 2015, in *IAU Symposium*, Vol. 307, *IAU Symposium*, 342–347
- Morel, T., Castro, N., Fossati, L., et al. 2014, *The Messenger*, 157, 27
- Moss, D. 2001, in *Astronomical Society of the Pacific Conference Series*, Vol. 248, *Magnetic Fields Across the Hertzsprung-Russell Diagram*, ed. G. Mathys, S. K. Solanki, & D. T. Wickramasinghe, 305
- Najarro, F., Hanson, M. M., & Puls, J. 2011, *A&A*, 535, A32
- Nazé, Y., Bagnulo, S., Petit, V., et al. 2012, *MNRAS*, 423, 3413
- Negueruela, I., Steele, I. A., & Bernabeu, G. 2004, *Astronomische Nachrichten*, 325, 749
- Neiner, C., Tkachenko, A., & MiMeS Collaboration. 2014, *A&A*, 563, L7
- Neubauer, F. J. 1943, *ApJ*, 97, 300
- Nieva, M.-F. & Przybilla, N. 2012, *A&A*, 539, A143
- Nieva, M.-F. & Przybilla, N. 2014, *A&A*, 566, A7
- Pedersen, H. & Thomsen, B. 1977, *A&AS*, 30, 11
- Petit, V., Massa, D. L., Marcolino, W. L. F., et al. 2011, *MNRAS*, 412, L45
- Petit, V., Owocki, S. P., Wade, G. A., et al. 2013, *MNRAS*, 429, 398
- Piskunov, N. & Kochukhov, O. 2002, *A&A*, 381, 736
- Piskunov, N., Snik, F., Dolgoplov, A., et al. 2011, *The Messenger*, 143, 7
- Piskunov, N. E., Kupka, F., Ryabchikova, T. A., Weiss, W. W., & Jeffery, C. S. 1995, *A&AS*, 112, 525
- Piskunov, N. E. & Valenti, J. A. 2002, *A&A*, 385, 1095
- Porter, J. M. & Rivinius, T. 2003, *PASP*, 115, 1153
- Press, W. H., Teukolsky, S. A., Vetterling, W. T., & Flannery, B. P. 1992, *Numerical recipes in FORTRAN. The art of scientific computing*
- Puls, J., Kudritzki, R., Herrero, A., et al. 1996, *A&A*, 305, 171
- Puls, J., Urbaneja, M. A., Venero, R., et al. 2005, *A&A*, 435, 669
- Puls, J., Vink, J. S., & Najarro, F. 2008, *A&A Rev.*, 16, 209
- Reed, B. C. 2003, *AJ*, 125, 2531
- Rivero González, J. G., Puls, J., Massey, P., & Najarro, F. 2012, *A&A*, 543, A95
- Rivinius, T., Szeifert, T., Barrera, L., et al. 2010, *MNRAS*, 405, L46
- Ryabchikova, T. A., Piskunov, N. E., Stempels, H. C., Kupka, F., & Weiss, W. W. 1999, *Physica Scripta Volume T*, 83, 162
- Salpeter, E. E. 1955, *ApJ*, 121, 161
- Sana, H., Le Bouquin, J.-B., Lacour, S., et al. 2014, *ApJS*, 215, 15
- Santolaya-Rey, A. E., Puls, J., & Herrero, A. 1997, *A&A*, 323, 488
- Schneider, F. R. N., Langer, N., de Koter, A., et al. 2014, *A&A*, 570, A66
- Simón-Díaz, S., Castro, N., Garcia, M., & Herrero, A. 2011a, in *IAU Symposium*, Vol. 272, *IAU Symposium*, ed. C. Neiner, G. Wade, G. Meynet, & G. Peters, 310–312
- Simón-Díaz, S., Castro, N., Herrero, A., et al. 2011b, *Journal of Physics Conference Series*, 328, 012021
- Simón-Díaz, S. & Herrero, A. 2014, *A&A*, 562, A135
- Simón-Díaz, S., Herrero, A., Esteban, C., & Najarro, F. 2006, *A&A*, 448, 351
- Simón-Díaz, S., Negueruela, I., Maíz Apellániz, J., et al. 2015, *ArXiv:1504.04257*
- Snik, F., Kochukhov, O., Piskunov, N., et al. 2011, in *Astronomical Society of the Pacific Conference Series*, Vol. 437, *Solar Polarization 6*, ed. J. R. Kuhn, D. M. Harrington, H. Lin, S. V. Berdyugina, J. Trujillo-Bueno, S. L. Keil, & T. Rimmele, 237
- Sota, A., Maíz Apellániz, J., Walborn, N. R., et al. 2011, *ApJS*, 193, 24
- Stahl, O., Wolf, B., Gang, T., et al. 1993, *A&A*, 274, L29
- Sundqvist, J. O., Petit, V., Owocki, S. P., et al. 2013, *MNRAS*, 433, 2497
- Thompson, G. I., Nandy, K., Jamar, C., et al. 1978, *Catalogue of stellar ultraviolet fluxes. A compilation of absolute stellar fluxes measured by the Sky Survey Telescope (S2/68) aboard the ESRO satellite TD-1*
- Tody, D. 1993, in *Astronomical Society of the Pacific Conference Series*, Vol. 52, *Astronomical Data Analysis Software and Systems II*, ed. R. J. Hanisch, R. J. V. Brissenden, & J. Barnes, 173
- Townsend, R. H. D. & Owocki, S. P. 2005, *MNRAS*, 357, 251
- Tutukov, A. V. & Fedorova, A. V. 2010, *Astronomy Reports*, 54, 156
- U, V., Urbaneja, M. A., Kudritzki, R., et al. 2009, *ApJ*, 704, 1120
- Ud-Doula, A., Owocki, S. P., & Townsend, R. H. D. 2009, *MNRAS*, 392, 1022
- Urbaneja, M. A., Herrero, A., Bresolin, F., et al. 2005, *ApJ*, 622, 862
- Vink, J. S., de Koter, A., & Lamers, H. J. G. L. M. 2000, *A&A*, 362, 295
- Wade, G. A., Grunhut, J., Alecian, E., et al. 2014, in *IAU Symposium*, Vol. 302, 265–269
- Wade, G. A., Grunhut, J., Gräfener, G., et al. 2012a, *MNRAS*, 419, 2459
- Wade, G. A., Maíz Apellániz, J., Martins, F., et al. 2012b, *MNRAS*, 425, 1278
- Walborn, N. R. 1972, *AJ*, 77, 312
- Walborn, N. R. 1980, *ApJS*, 44, 535
- Walborn, N. R. & Fitzpatrick, E. L. 1990, *PASP*, 102, 379
- Walborn, N. R. & Fitzpatrick, E. L. 2000, *PASP*, 112, 50
- Walborn, N. R. & Nichols, J. S. 1994, *ApJ*, 425, L29
- Walborn, N. R., Sota, A., Maíz Apellániz, J., et al. 2010, *ApJ*, 711, L143
- Wickramasinghe, D. T., Tout, C. A., & Ferrario, L. 2014, *MNRAS*, 437, 675

Table 1: Average longitudinal magnetic field values obtained from the FORS 2 and HARPS observations.

FORS 2									
Reduction	Date	HJD– 2450000	No. of frames	Exp. time (s)	S/N	$\langle B_z \rangle$ V (G) Hydrogen	$\langle B_z \rangle$ N (G)	$\langle B_z \rangle$ V (G) All	$\langle B_z \rangle$ N (G)
Bonn	07-Feb-2014	6696.7341	10	35	2359	-655 ± 109	22 ± 81	-504 ± 54	69 ± 46
Potsdam						-639 ± 121	-16 ± 119	-460 ± 65	76 ± 66
Bonn	08-Feb-2014	6697.7162	10	30	2398	-978 ± 88	-36 ± 76	-653 ± 47	40 ± 43
Potsdam						-877 ± 91	-102 ± 105	-521 ± 62	23 ± 63
HARPS									
Reduction	Date	HJD– 2450000	No. of frames	Exp. time (s)	S/N	$\langle B_z \rangle$ V (G)	Detection	FAP	
Bonn (LSD)						-592 ± 7	DD	$< 10^{-15}$	
Potsdam (SVD)	23-Apr-2014	6770.4993	4	2700	347	-583 ± 9	DD	$< 10^{-16}$	
Potsdam (MT)						-584 ± 15	-	-	

Notes. Column 1 indicates the group that performed the data reduction and analysis, which led to the results shown in the following columns. The heliocentric Julian date shown in Col. 3 indicates the beginning of the sequence of exposures. Column 4 gives the number of frames obtained during each night of observation and Col. 5 the exposure time of each frame. Column 6 gives the S/N per pixel of Stokes I calculated at about 4950 Å over a wavelength range of 100 Å. In the FORS 2 subtable, Cols. 7 and 8 give the $\langle B_z \rangle$ values obtained using the spectral regions covered by the hydrogen lines obtained from the Stokes V and N parameter spectrum, respectively. The same is given in Cols. 9 and 10, but using the full spectrum (see Sect. 3.1). In the HARPS subtable, Cols. 7 and 8 give the $\langle B_z \rangle$ V values and the detection flag (DD, definite detection). Column 9 gives the false alarm probability (FAP) for those methods that provide it. The different detection techniques are listed in Col. 1 (see Sect. 3.2).

Table 2: Stellar parameters and chemical abundances of HD 54879 and of the O9.7 V standard star HD 36512 (Sota et al. 2011).

ID	Instrument	T_{eff} (K)	$\log g$ (dex)	$\log Q$	ξ^b (km s ⁻¹)	He/H (by number)
HD 54879	FORS 2	33000 ± 1000	3.95 ± 0.10	- ^{a)}	5 ± 3	$0.10 - 0.12$
	HARPS	33000 ± 1000	4.00 ± 0.10	- ^{a)}	4 ± 1	$0.10 - 0.12$
HD 36512	FIES	33400 ± 600	4.09 ± 0.11	-13.46	10	0.10
		$\log \epsilon_{\text{Si}}$	$\log \epsilon_{\text{Mg}}$	$\log \epsilon_{\text{C}}$	$\log \epsilon_{\text{N}}$	$\log \epsilon_{\text{O}}$
HD 54879	FORS 2	7.3 ± 0.3	7.4 ± 0.3	7.8 ± 0.3	7.5 ± 0.3	8.6 ± 0.2
	HARPS	7.4 ± 0.2	7.4 ± 0.1	8.1 ± 0.2	7.7 ± 0.2	8.6 ± 0.1
☉		7.51	7.60	8.43	7.83	8.69
CAS		7.50	7.56	8.33	7.79	8.76

Notes. *a)* The parameter $Q = \dot{M} / (R_* v_\infty)^{1.5}$ (Puls et al. 1996) relies mainly on the Balmer lines, which for HD 54879 are not suitable for setting the mass-loss rate (Sect. 4). *b)* Microturbulence. The solar abundances (☉) are taken from Asplund et al. (2009). The cosmic abundance standard (CAS) composition from Nieva & Przybilla (2012) is also listed, $\log \epsilon_{\text{X}} = \log (X/H) + 12$ (by number).

Appendix A: HARPS best-fit modelling

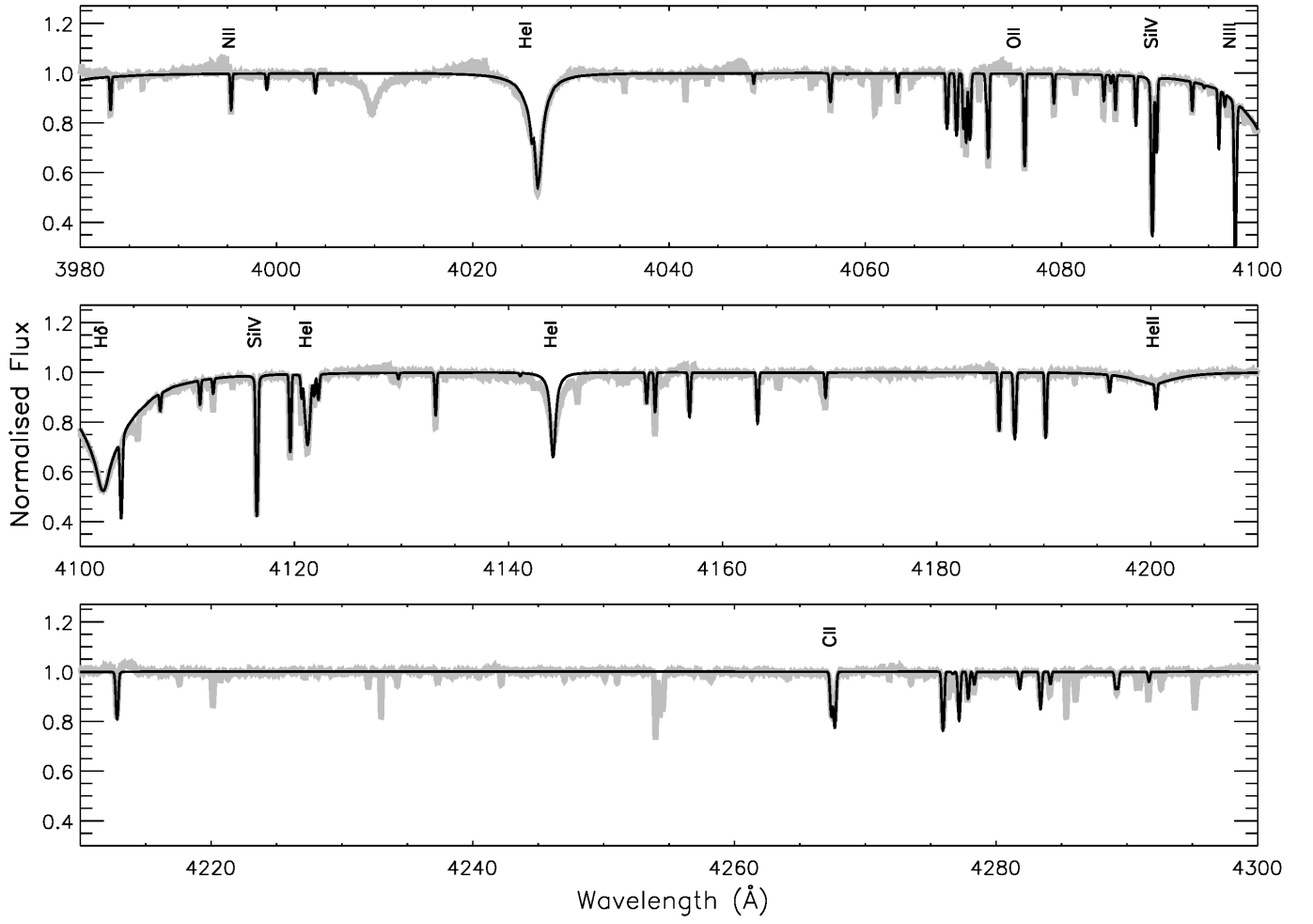


Fig. A.1: Normalised optical spectrum (grey) and the best-fit FASTWIND stellar model (black), see Fig. 7.

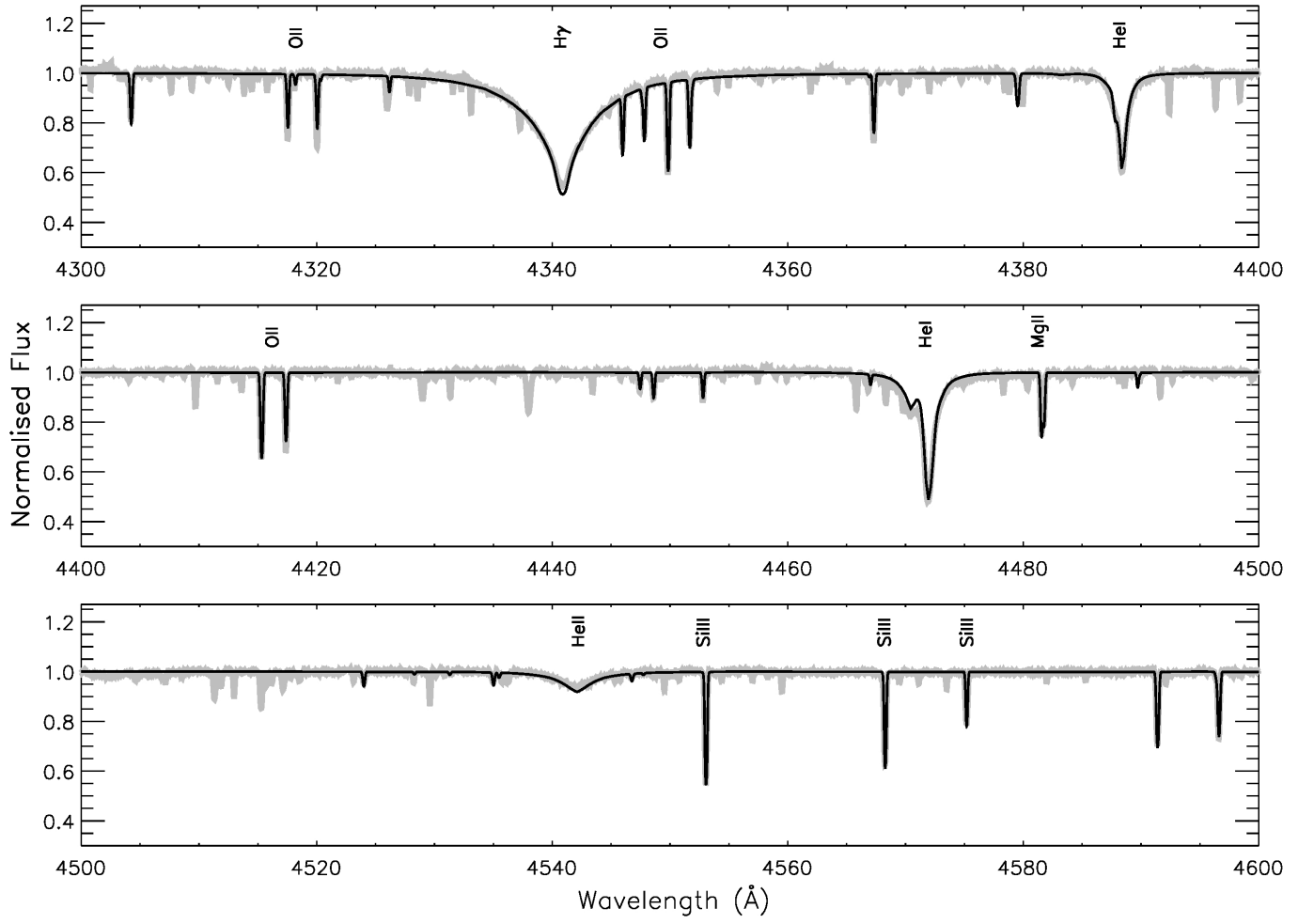


Fig. A.2: Figure A.1 continued.

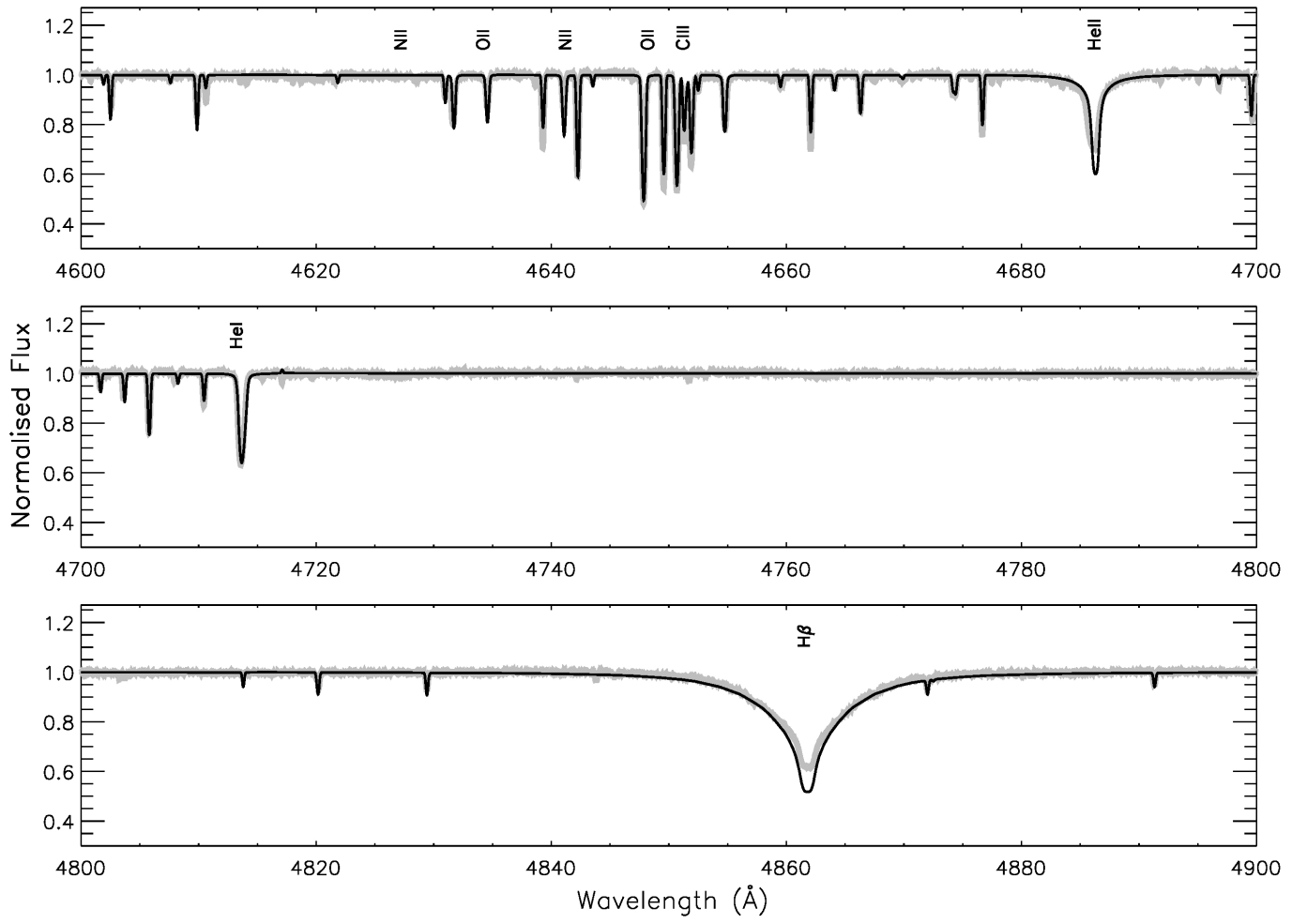


Fig. A.3: Figure A.1 continued.